Numerical Simulation of Vortex Shedding at Triangular Obstacle for Various Reynolds Numbers and Times with Open FOAM

Ahmad Jafari, Seyyedeh Zahra Malekhoseini

***Abstract*— The present study aimed to simulate the two-dimensional flow around a triangular obstacle in a channel. Numerical study was performed by the open-source numerical model, OpenFOAM. IcoFoam solver was used to solve the equations governing the flow in the modeling. The Navier-Stokes and continuity equations are the dominant equations in this solver. In the first step, flow lines and velocity vectors were simulated for Reynolds numbers of 20, 30 and 35. The simulations showed that the separation of flow lines and the formation of vortex bubbles depend on the Reynolds number, even when this parameter slightly increases. In the second step, the flow lines at six different times with the time interval t/6 at Reynolds numbers of 150 and 200 were identified. Based on the results, it was indicated that only at the time of 150s a different pattern was observed for the flow lines. In the third step, as the Reynolds number increases, changes in the flow lines pattern were studied in a regime with Reynolds numbers of 4, 35, 70, 120 and 200, resulting in turbulence in the flow lines. To measure numerical stability during processing, the average and maximum values of Courant number were calculated at every stage of solution and implementation. The residual and velocity changes graphs were depicted based on location in the x-y plane to analyze the data. Finally, based on the verified results, the ability and power of the numerical model was evaluated and It is concluded that as an appropriate efficient model in this field.**

***Index Terms*— OpenFOAM, Reynolds number, vortex, triangular obstacle, numerical model.**

I. INTRODUCTION

Hydraulic structures built along streams are used for different purposes such as drinking, farming, etc. By building the structures across the flow of water, flow lines are changed and vortices are formed downstream. This phenomenon is involved in various issues such as erosion and sedimentation, structural stability and even energy production from downstream vortices. The clean energy produced by vibrations of vortices on the downstream side of obstacles is regarded as a renewable energy source [1]. To produce vibrations, it is necessary to place obstacles perpendicular to the flow path [2]. High-pressure fluid near the edges develops the boundary layer on both sides of the obstacle. Regarding the separation pattern of flow lines, they are separated at both side edges of the obstacle and shear layers are formed sequentially in the downstream direction creating a wake region. The outer shear layers generate discontinuous rotational movements and create a regular pattern of vortices in the wake region (Figure 1). Rajani et al. simulated an unsteady laminar flow downstream of an obstacle using the open-source model OpenFOAM [3]. As a result, length of the wake region was reduced and the flow separation point was changed in the small gap between the side wall and the obstacle. Wei et al. simulated and analyzed vortex-induced vibrations for a circular obstacle using the numerical model OpenFOAM [4]. The results of this numerical model were similar to those obtained from experimental data. Roohi et al. examined the backflow downstream of an obstacle using the numerical model OpenFOAM and the extended finite volume method [5]. By comparing the results of the numerical model with those obtained from other models, high processing power of this model was highlighted in this field. Luo and Tan [6] generated parallel vortices in the flow regime with high Reynolds numbers using the end suction of obstacle and measured the associated aerodynamic parameters. Reynolds number is one of the basic parameters in defining the vortices, and many studies on vortex-induced vibrations were conducted at critical and sub-critical Reynolds numbers [7]. De and Dalal simulated the flow downstream of an obstacle at low Reynolds numbers using the numerical model and showed that flow oscillations are depend on the dimensionless parameter of Reynolds number [8]. Wanderley and Soares highlighted the crucial role of Reynolds number on the lift coefficient, oscillation amplitude, and oscillation frequency [9]. When the vortex-induced frequency (Fs) equals to the natural frequency of oscillations, resonance occurs [10]. Waves with maximum amplitude are generated under the resonance conditions [11]. Resonance conditions are the optimum conditions for extraction of the maximum energy. Badhurshah and Samad [12], Tongphong and Saimek [13], Okuhara et al. [14], and Setoguchi et al. [15] conducted studies on how to build generators (turbines) with maximum efficiency for extraction of energy from vortex-induced waves. Vortex shedding in a porous structure depends on the shape and thickness of the obstacle. As the obstacle become thicker and sharper, vortex shedding phenomenon is more aggravated [16]. In an experimental and numerical study, impacts of the cross-sectional shape of the obstacle on the wave amplitude and energy extracted from vibrations were investigated. The maximum efficiency of energy harvesting for obstacles with circular and trapezoidal cross-sections were equal to 45.7% and 37.9%, respectively. [17]. Jafari et al. observed ten transverse waves induced by vortices in an experimental study and stated that the amplitude ratio of the produced waves is a function of the vertical and horizontal distance from obstacles, Strouhal number, Reynolds number, the number of obstacles, and the wave number [18]. They also proposed relations for

Ahmad Jafari,, Department of Water Engineering, Ramin Agriculture and Natural Resources University of Khuzestan, Iran

Seyyedeh Zahra Malekhoseini[2], Former MSc Student, Department of Water Engineering, Ramin Agriculture and Natural Resources University of Khuzestan, Iran

the amplitude ratio of waves in linear and scattered configurations of obstacles. The results of the experimental study on ten modes of transverse waves include observation of wave modes by reducing the depth of the mainstream, creating waves under submerged flow conditions on the obstacle, and observation of the maximum amplitude with the size equivalent to 40% of the flow depth [19]. Ghomeshi et al. examined the impact of obstacles configuration on the wave modes and concluded that in every wave mode, wave amplitude increases as the obstacles row spacing reduces [20]. Strouhal number is another dimensionless parameter affecting the vortex shedding phenomenon which is correlated to frequency of vortices. In fact, as a result of the correlation between these two parameters, vortex shedding is of the most important phenomena fluid mechanics. Fluid flow over obstacles induces vortices with certain frequencies. These frequencies can be calculated using the relations proposed by the researchers.

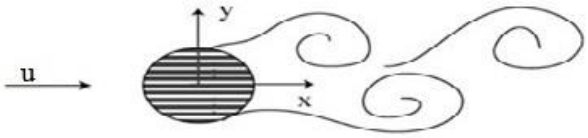

Figure 1- Vortex shedding when the fluid flows over an obstacle

Blevins [21], Harris and Peirsol [22], and Leinhard [23] specified vortex pattern over a wide range of Reynolds numbers. Vortex shedding is a phenomenon under study in many fields of engineering. Besides the damaging effects, studies and solutions to control this phenomenon against aggravation and provide its creation conditions to extract energy were presented. This phenomenon induces vibration of structures [24], increases fluid resistance [25] and creates noise [26]. For example, the effects of magnetic field and properties of porous materials on control, formation and suppression of wakes were identified in a numerical study. The results of this study include reduction in length of wakes with the increase of Darcy number, vortices controlled by the magnetic field for small Darcy numbers, and reduction in Stewart number with increasing Darcy number [27]. Chen and Shaw presented vortex control test results under the conditions of an element in a specific area entitled "effective area" [28]. Dipankar et al. [29], Zhu et al. [30], and Mittal and Raghuvanshi [31] conducted studies on control of vortices over the range of low Reynolds numbers using a numerical model and offered solutions such as locating a control cylinder or plane at a specific distance from obstacles. Perumal et al. simulated the vortex shedding phenomenon using the Lattice Boltzmann method in a two-dimensional numerical study [32]. In this study, they examined the effects of Reynolds number, blockage ratio, and channel length on the phenomenon and concluded that flow is stable at low Reynolds numbers and a pair of symmetric static vortices is formed behind the obstacle. Abdolahi and Atefi analyzed this phenomenon using the Lattice Boltzmann method and reported the results such as creation of a flow without any separation over the range of Reynolds numbers less than 1, flow separation over the range of Reynolds numbers greater than 3, and formation of a steady flow with symmetric vortices, vortex shedding phenomenon, non-permanent behavior at Reynolds numbers greater than 55, and penetration of vortex flow from behind the obstacle towards the front edge over the range of Reynolds numbers greater than 130 [33]. In the present study, considering the importance of the issues mentioned on the fluctuating flows, collision of the flow with the obstacles was analyzed. At each step of modeling, the details of the flow behavior in the corresponding regime were analyzed by examination of flow lines and velocity vectors, and the results were validated by comparison of the previous studies. It should be noted that in most studies referred in this regard, the tested fluid was gas but in the present study water was considered as the testing fluid.

II. Material and Methods

The present study aimed to simulate vortex pattern on the downstream side of a triangular obstacle using the Open Source Field Operation and Manipulation and examining the details for various regime conditions. For this purpose, tests were carried out in several steps and the results were presented. The numerical model OpenFOAM is a computational fluid dynamics tool capable of modeling any kind of problems such as partial differential equations including numerical solution of fluid flow from simple to very complex problems. Examples of cases that can be modeled by this software include problems related to laminar and turbulent flows, single-phase and multi-phase, heat transfer, chemical reactions, electromagnetic, solid mechanics, and economic equations. Flexible and efficient kernel of the software includes a set of codes written in C ++. IcoFoam solver was used to solve the equations governing the flow in the modeling. The name of solver was derived from the type of fluid used in it, i.e. incompressible fluid. This solver can be used to solve an unsteady laminar flow for an incompressible Newtonian fluid. The Navier-Stokes and continuity equations are the dominant equations in this solver. The general form of the continuity equation for incompressible flow is expressed by Equation 1 [34]. The law of conservation of energy is shown by the energy equation (Equation 2). The law of motion may be expressed by the Navier-Stokes equation (Equation 3). In these equations, h represents enthalpy (heat content of the system at a constant pressure), c is thermal conductivity, T represents temperature, (i, j = 1,2,3) are tensors of the summation index, m represents dynamic viscosity, P represents pressure, δ_{ij} represents the Kronecker delta function (if i and j are equal, δ_{ij} is one, and if $i \neq j$, δ_{ij} is zero), λ represents volume viscosity coefficient which is only related to volume expansion, u shows velocity, and Fi shows external body forces such as gravity and electromagnetic fields [35].

$$\frac{\partial U_i}{\partial x_i} = 0 \tag{1}$$

$$\left(\frac{Dh}{Dt}\right) = \frac{DP}{Dt} + \frac{\partial}{\partial x_j}\left(c\,\frac{\partial T}{\partial x_j}\right) + \mu\left(\frac{\partial U_i}{\partial x_j} + \frac{\partial U_j}{\partial U_i}\right)\frac{\partial U_i}{\partial x_j} \tag{2}$$

$$\rho\left(\frac{\partial U_i}{\partial t} + U_j\left(\frac{\partial U_i}{\partial x_j}\right)\right) = -\frac{\partial P}{\partial x_i} + \frac{\partial}{\partial x_j}\left(\mu\left(\frac{\partial U_i}{\partial x_j} + \frac{\partial U_j}{\partial U_i}\right) + \lambda\delta_{ij}\frac{\partial U_i}{\partial x_i}\right) + F_i \tag{3}$$

Simulation of vortices on the downstream side of a triangular obstacle at Reynolds numbers of 20, 30 and 35 was the first step in the present study. In this step, it was necessary to determine geometry of the problem, plot and mesh it in Gambit software and then use it in the numerical model. Figure 2 shows geometry of the problem in the first step. For this geometry, blockage ratio (h/ H), Xu / h, and Xd / h were considered to be 20, 9, and 20, respectively.

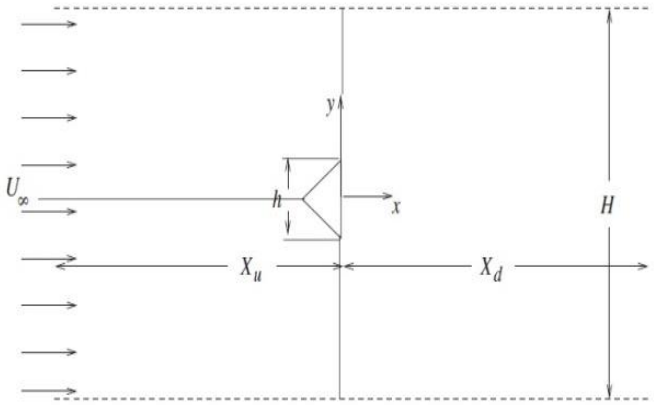

Figure 2- geometry of the problem

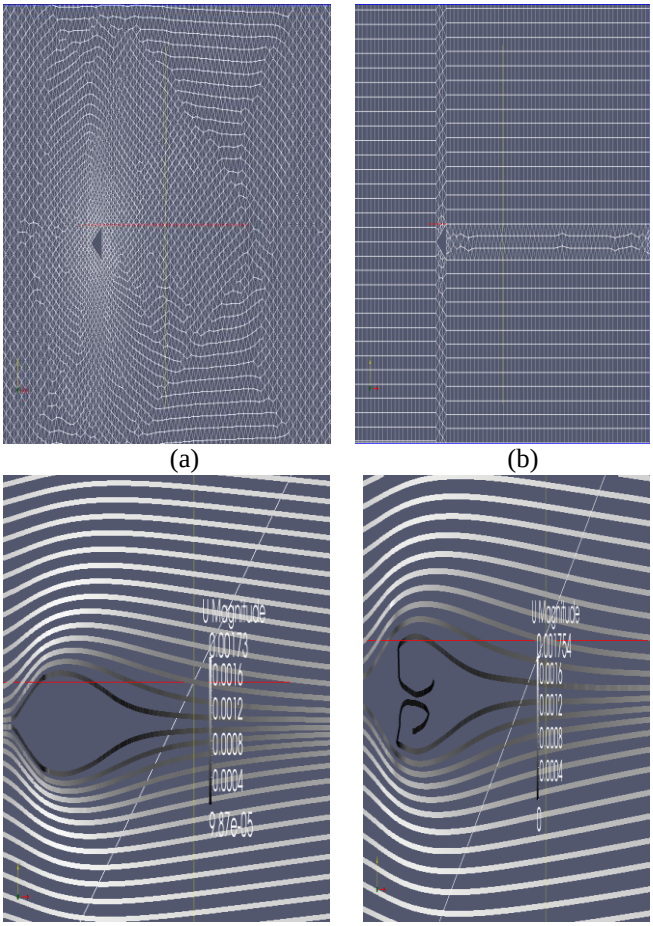

Figure 3- The meshes generated in Gambit software

Mesh quality in Gambit software is one of the parameters affecting the simulation results. Figure 3 (a) represents meshing with triangular element of pave-type. In Figure 3 (b) geometry of the problem is divided to 6 areas in which three areas are meshed with regular structure and square elements of map-type and the three other areas are meshed along the sides of the obstacle with irregular structure and triangular element of pave-type. The outcomes of both meshes related to the flow lines at Reynolds number 35 are presented in parts (c) and (d). As De and Dalal indicated symmetric vortex pairs are formed at downstream of the obstacle at Reynolds number 35 [8]. These two vortices are only quite clear through the back flow lines on the mesh shown in part (b). Accordingly, the mesh shown in part (b) was selected. Also, some tests were performed on the number of meshes in part (b) (Table 1). As it is indicated, as the number of meshes increases, the outcome become better and sharper (Figure 4). The closest result to the results obtained by De and Dalal at Reynolds number 35 was related to meshing with m=0.01 and n=0.004. As a result, meshing with these characteristics was selected as the best meshing in this study (Figure 4 (d)).

Table 1- The number of nodes in an irregular mesh

Mesh size for the first layer around the obstacle (n)	0.01	0.008	0.006	0.004
Mesh size for the end layers (m)	0.07	0.05	0.03	0.01

To set velocity boundary conditions in the numerical model, its value was calculated using equation 4, where h represents the base length of the triangular obstacle and at every step, the initial velocity equaled to this value due to the velocity gradient which equals to zero. Pressure boundary conditions were set in the corresponding folder with the initial value of 1 atmosphere, due to the pressure gradient equaled to zero. Table 2 shows a report on the required and determined conditions in this step. In this table, Re is Reynolds number (dimensionless parameter), and U is flow velocity (meters per second). Also, D represents the side length of the square obstacle (0.0251 m), υ represents kinematic viscosity (1.004*10-6 m2/s), and P represents pressure (1 atmosphere). The entire process of modeling was conducted at the temperature of 25 ° C. The initial conditions for the solution including start time, end time, output time interval, and iteration step, were set in the corresponding file. To have a good time step and numerical stability during processing the Courant number should be less than 1. In the equation 5, C0 is the Courant number, U is absolute velocity of the cell, Δx is the cell size along the velocity and Δt is time step. Cell sizes can be calculated by the equation 6. Where, d is the path length along the velocity, and n is the number of cells generated along the length. All tests in this step were conducted with an end time of *300 s and ⊿t= 0.2 s.*

$$Re = \frac{U \times h}{\upsilon} \qquad (4)$$

$$C_0 = U\frac{\Delta t}{\Delta x} \qquad (5)$$

$$\Delta x = \frac{d}{n} \qquad (6)$$

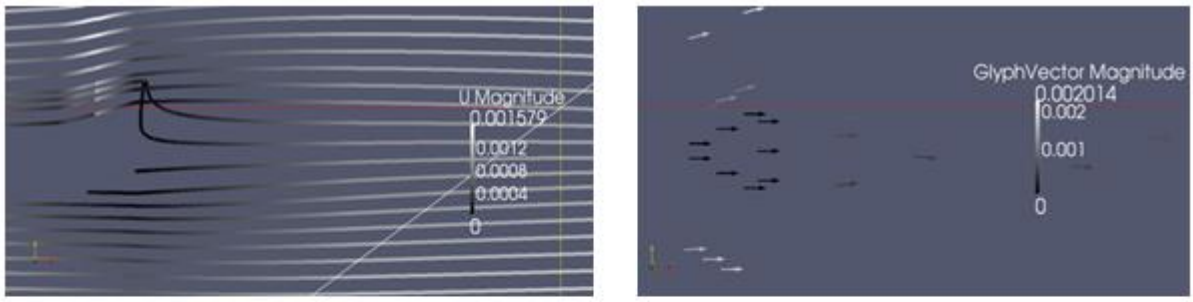

a. n= 0.01, m=0.07

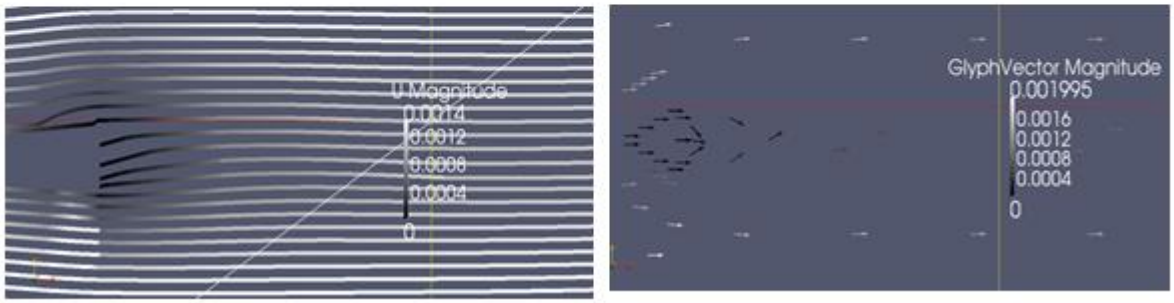

b. n= 0.008, m=0.05

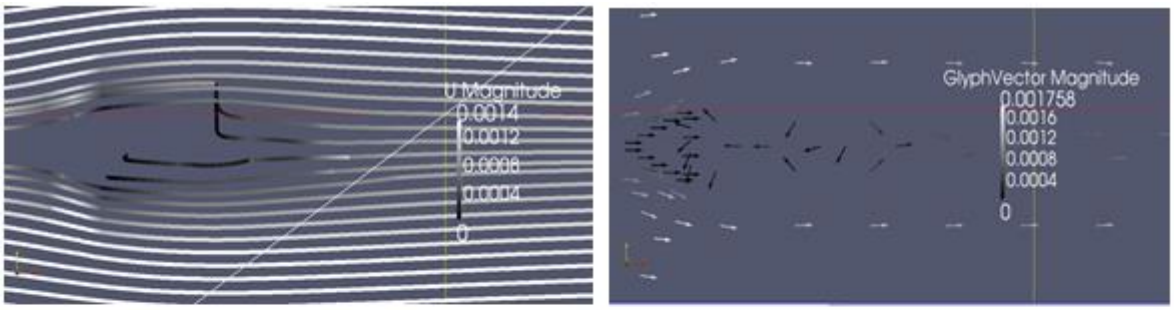

c. n= 0.006, m=0.03

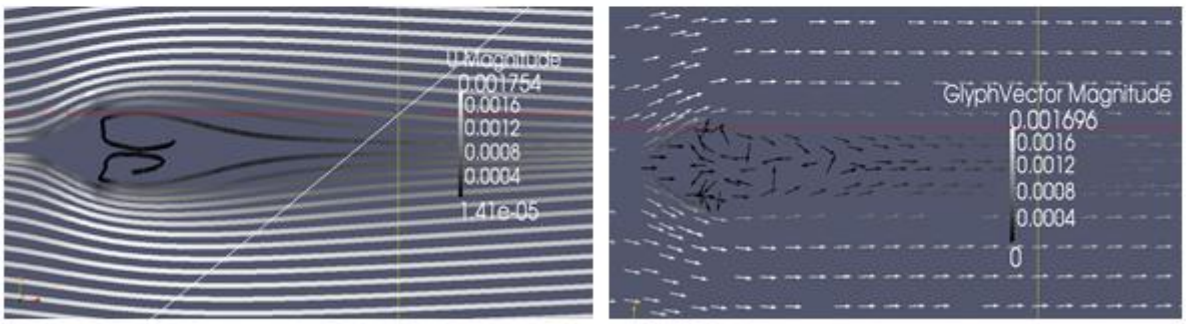

d. n= 0.004, m=0.01

Figure 4- Flow lines and velocity vectors for different mesh sizes at Reynolds number 35

Then, by writing name of the solver in the terminal, modeling started and the results of solving steps such as the Courant number, residual, and accuracy of convergence were seen in the terminal. This model uses the finite volume numerical method to solve partial differential equations, in which multi-faceted cells are attributed to each non-structured three-dimensional mesh. Residuals usage is one of the methods to estimate error in solving the governing equations. During the modeling, the aforementioned values are calculated by the model and displayed in the terminal. Finally,

the results can be observed in the post-processing software, ParaView. Due to the large number of observational results in the terminal, only a few details within the selected time step at Reynolds number 30 were presented in Table 3. In this table, T represents time (s), C0 represents the Courant number, MaxC0 represents the maximum Courant number, U represents the flow velocity (meters per second), I.res U represents the residual of the primary solution for velocity in the corresponding direction, F.res U represents the residual of the final solution for velocity in the corresponding direction, Iter U represents number of iterations for velocity in the corresponding direction, I.res P represents the residual of the primary solution for pressure, F.res P represents the residual of the final solution for pressure, and Iter P represents number of iterations for pressure.

The second step focused on the study of vortices at Reynolds numbers of 150 and 200 in different times, and comparison of the created patterns. Details are presented below. This step of simulation was conducted with the same geometry as before. Reports of the solving results observed in the terminal for Reynolds numbers of 150 and 200 are presented in Tables 4 and 5 for the last steps. All solution settings were considered the same as the previous step. The end time of 300 s and Δt equal to 0.5 s were considered for the tests in this step. As mentioned above,, the Courant number should be less than 1 to perform an approved modeling. This is indicated by the column C0 in all three tables. In the third step, changes in the pattern of vortex shedding at Reynolds numbers of 4, 35, 70, 120 and 200 were studied. All the necessary measures in this step were performed same as the previous two steps.

Table 2- Boundary conditions and effective parameters in the first step

Re	U(m/s)
20	0.0008
30	0.0012
35	0.0014

Table 3- The observational results of the icoFoam solver in the terminal at Reynolds number 30

T(s)	C_0	Max C_0	U (m/s) $\times 10^3$	I.res $U_x \times 10^4$	F.res $U_x \times 10^8$	IterU_x	I.res $U_y \times 10^4$	F.res $U_y \times 10^8$	IterU_y	I.res $P \times 10^5$	F.res $P \times 10^7$	Iter P
298.8	0.013	0.173	1.424	1.379	1.486	1	2.669	1.025	1	3.123	9.733	46
299	0.013	0.173	1.424	1.922	1.493	1	2.667	1.025	1	3.134	7.308	27
299.2	0.013	0.173	1.424	1.921	1.499	1	2.665	1.025	1	3.129	8.122	47
299.4	0.013	0.173	1.424	1.919	1.505	1	2.664	1.025	1	3.154	7.362	27
299.6	0.013	0.173	1.424	1.918	1.511	1	2.662	1.025	1	3.207	7.72	47
299.8	0.013	0.173	1.424	1.917	1.519	1	2.659	1.024	1	3.58	8.027	27
300	0.013	0.173	1.424	1.916	1.524	1	2.658	1.025	1	3.915	8.687	48

Table 4- The observational results of the icoFoam solver in the terminal at Reynolds number 150

T(s)	C_0	Max C_0	U (m/s) $\times 10^3$	I.res $U_x \times 10^2$	F.res $U_x \times 10^6$	IterU_x	I.res $U_y \times 10^2$	F.res $U_y \times 10^7$	IterU_y	I.res $P \times 10^2$	F.res $P \times 10^7$	Iter P
297	0.175	1.761	7.625	1.364	2.981	2	3.755	5.244	3	5.397	8.838	76
297.5	0.175	1.762	7.633	1.359	3.083	2	3.769	6.176	3	5.612	9.218	77
298	0.175	1.763	7.67	1.357	3.135	2	3.779	7.098	3	5.681	8.489	86
298.5	0.175	1.765	7.691	1.358	3.188	2	3.788	7.808	3	5.154	8.516	79
299	0.175	1.767	7.71	1.358	3.275	2	3.801	8.329	3	5.386	8.131	77
299.5	0.175	1.768	7.725	1.354	3.279	2	3.82	8.677	3	5.526	9.771	76
300	0.175	1.771	7.734	1.352	3.227	2	3.838	8.859	3	5.511	9.56	77

Table 5- The observational results of the icoFoam solver in the terminal at Reynolds number 200

T(s)	C_0	Max C_0	U (m/s) $\times 10^2$	I.res $U_x\times 10^2$	F.res $U_x\times 10^6$	IterU_x	I.res $U_y\times 10^2$	F.res $U_y\times 10^6$	IterU_y	I.res P$\times 10^2$	F.res P$\times 10^7$	Iter P
297	0.234	2.481	1.025	1.678	7.647	2	4.666	2.218	3	5.691	9.463	76
297.5	0.234	2.481	1.022	1.689	7.868	2	4.66	2.06	3	5.59	8.837	77
298	0.234	2.481	1.018	1.694	7.881	2	4.666	3.778	3	5.36	8.342	74
298.5	0.234	2.481	1.018	1.697	7.713	2	4.648	6.088	3	5.436	9.152	72
299	0.234	2.48	1.017	1.709	6.659	2	4.625	7.841	3	5.395	9.68	84
299.5	0.234	2.478	1.014	1.71	5.826	2	4.624	7.348	3	5.52	6.51	69
300	0.234	2.477	1.009	1.712	5.158	2	4.607	4.136	3	5.982	9.735	75

III. Results

In this section, the validated results of all tests were presented and examined. To analyze data, graphs were depicted that are explained in the following. Figure 5 (a) and (b) show velocity vectors and flow lines around a triangular obstacle at Reynolds number 20, respectively. According to shape of the flow lines, it can be said that separation of the flow lines and backflow occurred in these circumstances. De and Dalal observed symmetric pairs of small vortices behind the obstacle by simulating the same conditions (Figure 4 c) [8]. Figure 6 (a) and (b) showed velocity vectors and flow lines at Reynolds number 30, respectively. According to direction of the velocity vectors, the symmetric vortex pairs can be seen. Backflow also occurred in the flow lines but not entirely. In similar conditions, De and Dalal observed symmetric vortex pairs behind the triangular obstacle at Reynolds number 30 shown in Figure 6 (c) [8]. Based on the results of their study, the vortex pairs created in these conditions were bigger than the vortex pairs in the previous conditions. Figure 7 (a) and (b) showed velocity vectors and flow lines at Reynolds number 35, respectively. In this section, pattern of flow lines and velocity vectors were the same as the regime with Reynolds number 30, but backflows were more complete and a slight increase can be seen in the size of the symmetric vortex pairs fixed behind the obstacle. De and Dalal simulated pattern of flow lines at Reynolds number 35, Figure 7 (c), which are in accordance with the results of the present study [8]. In the second step of the present study, pattern of flow lines was analyzed at Reynolds numbers of 150 and 200 and then compared at six different times. Figure 8 (a) showed patterns created with time steps of t =6 s for Reynolds number 150, and Figure 8 (a) showed the patterns for Reynolds number 200. At the time of 50 s, the patterns were the same and backflow lines and vortex pairs can be seen. At the time of 50 s, symmetry of vortex pairs was considerable only for the regime with Reynolds number 150. At the time of 100 s, similar patterns were created in the two conditions but at this time, the vortex pairs were bigger than the previous time. At the time of 100 s, symmetry of vortex pairs was considerable in both conditions. At 150 s, asymmetric vortex pairs were formed at Reynolds number 150. However, at Reynolds number 200, flow lines separation was formed with the alternative recirculation zone to the downstream. At 200 s, quite similar patterns to the case of alternative recirculation zone were formed. At 250 s and 300 s, alternative recirculation zone was formed in both conditions with negligible differences. De and Dalal also compared the patterns created in six time steps at Reynolds numbers of 150 and 200 (Figure 9) [8]. The results indicated full similarity of the patterns in all time steps, and only the results at 150s were not consistent with the results of the present study.

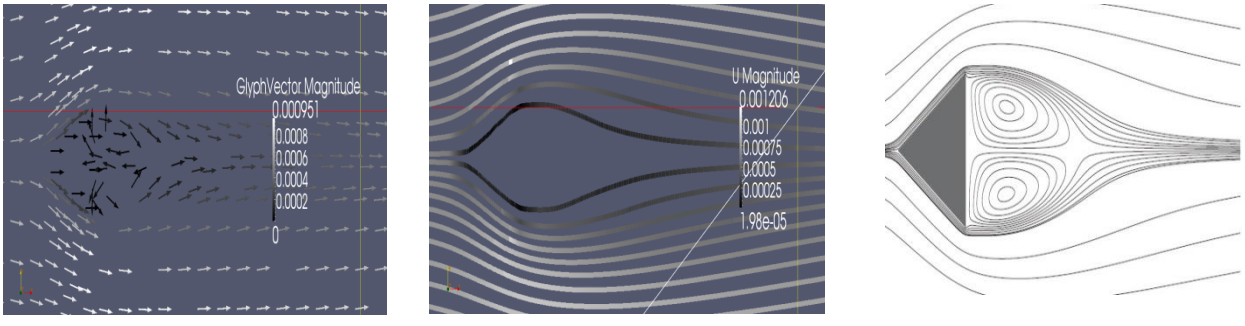

(a) (b) (c)

Figure 5- Simulation of flow around a triangular obstacle at Reynolds number 20
a) Flow lines in the present study. b) Velocity vectors in the present study. c) Vortex pattern [8]

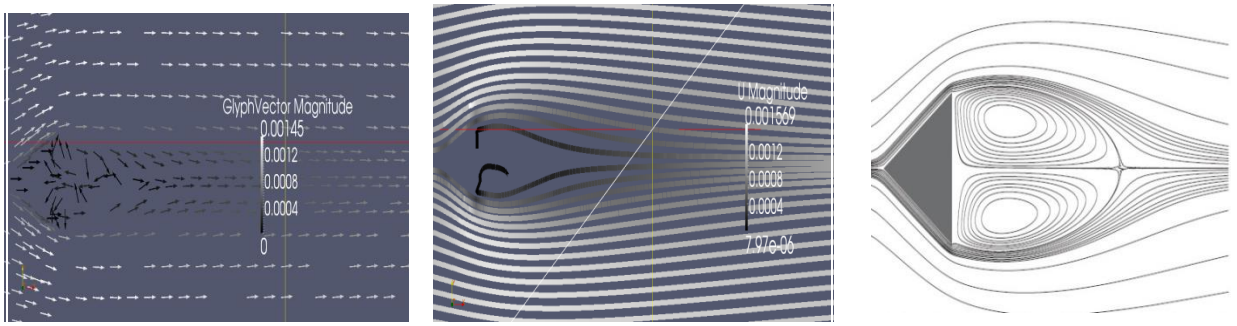

(a) (b) (c)

Figure 6- Simulation of flow around a triangular obstacle at Reynolds number 30
a) Flow lines in the present study. b) Velocity vectors in the present study. c) Vortex pattern [8]

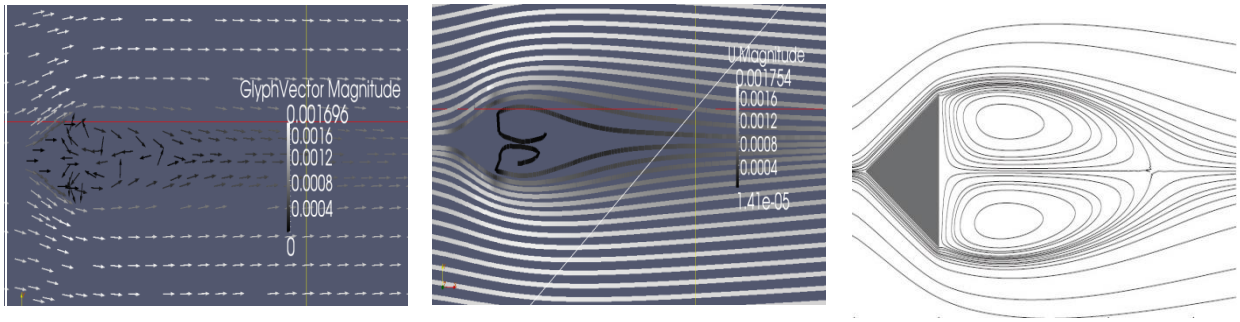

(a) (b) (c)

Figure 7- Simulation of flow around a triangular obstacle at Reynolds number 35
a) Flow lines in the present study. b) Velocity vectors in the present study. c) Vortex pattern [8]

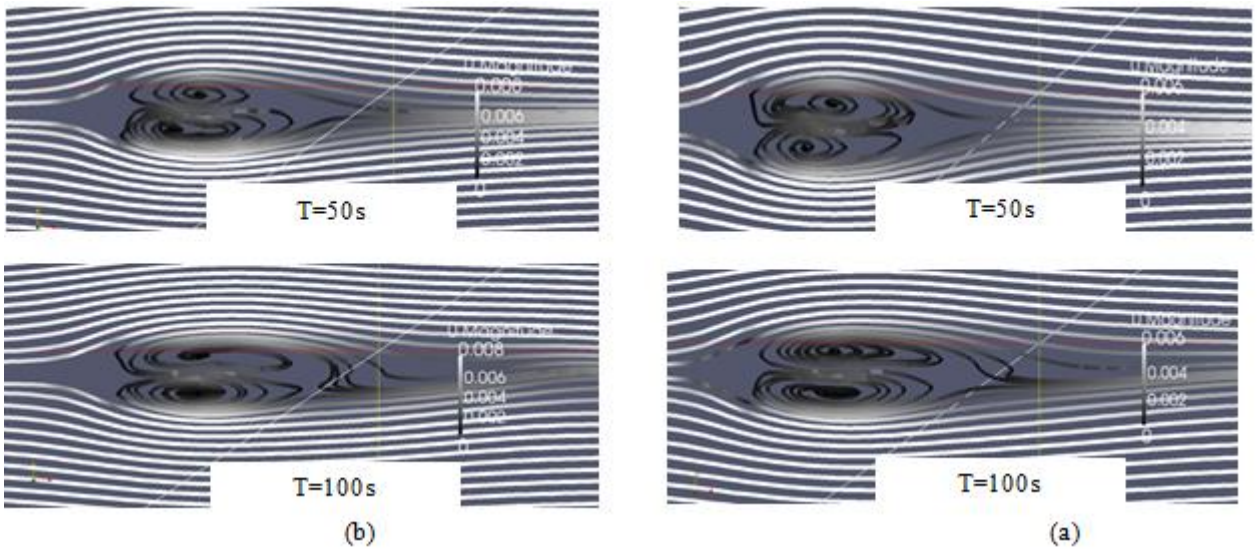

Figure 8- Vortex pattern in time step T/6. a) At Reynolds number 200. b) At Reynolds number 150

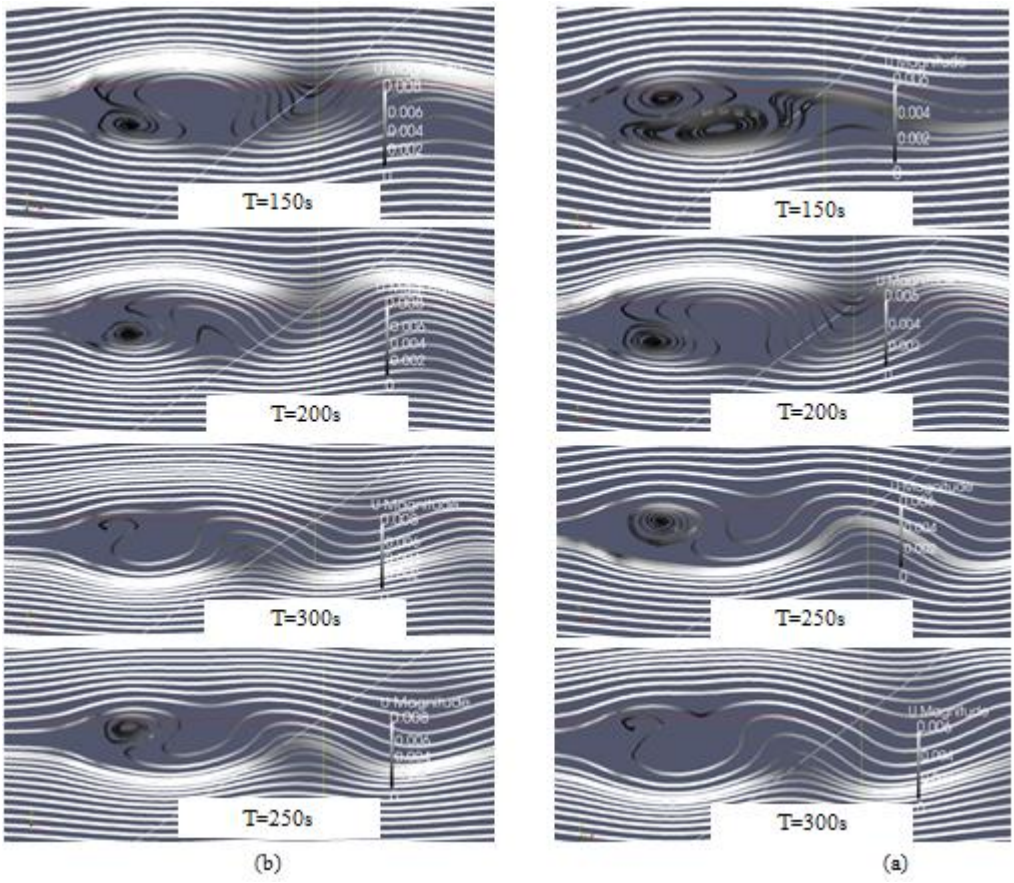

Figure 8 (Continue)- Vortex pattern in time step T/6. a) At Reynolds number 200. b) At Reynolds number 150

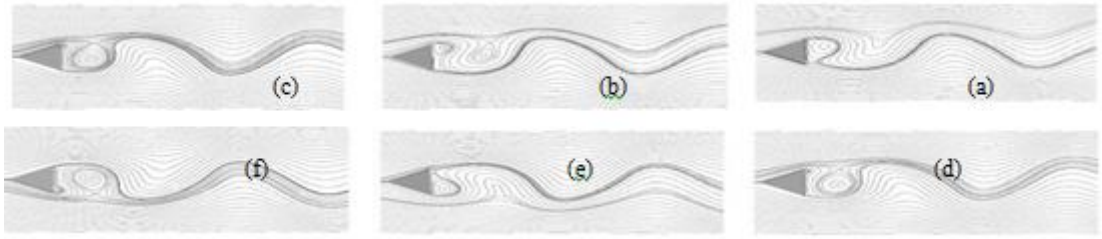

Figure 9- Vortex pattern in time step T / 6 at Reynolds numbers of 150 and 200 [8]

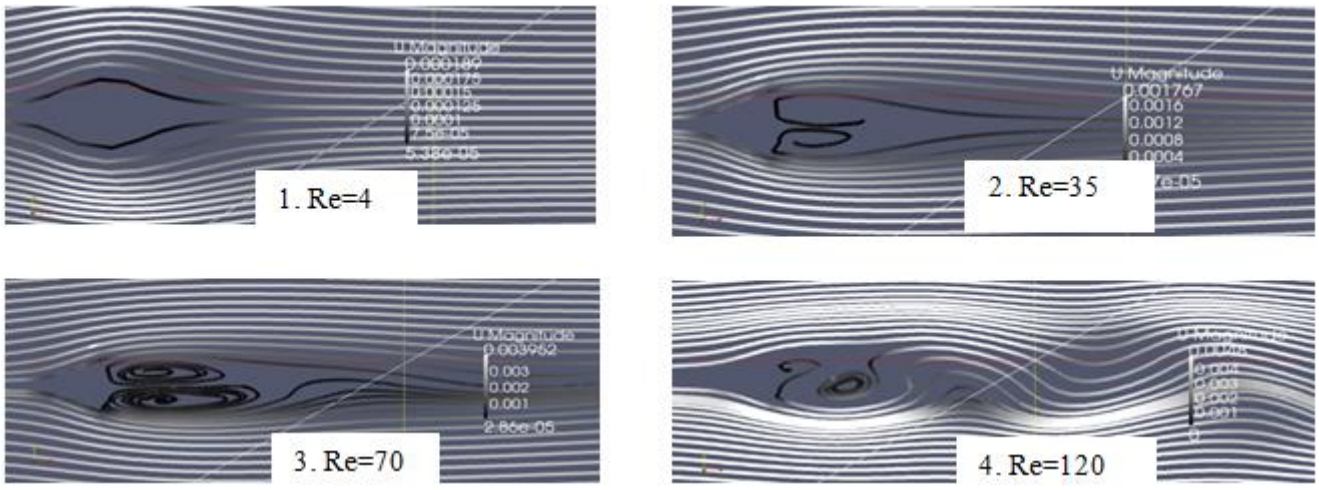

Figure 10- Flow patterns at Reynolds numbers of 4, 35, 70 and 120

The third step of the present study aimed to investigate changes in the flow line pattern with increasing the Reynolds number. Figure 10 illustrates these patterns at Reynolds numbers of 4, 35, 70 and 120. Figure 10.1 shows flow line pattern at Reynolds number 4 and as can be seen, no flow line separation occurred. Figure 10.2 shows flow line pattern at

Reynolds number 35. Formation of vortex bubbles behind the cylinder can be observed in these conditions due to back flow lines. Figure 10.3 shows flow line pattern at Reynolds number 70 and as can be seen, asymmetric vortex bubbles were formed in these conditions and number of back flow lines was more than the previous conditions. Figure 10.4 shows flow line pattern at Reynolds number 120, where vortex bubble separation occurred and the alternative recirculation zone to the downstream was observed. At every step, graphs were plotted to analyze data using the numerical model including velocity versus position graphs and residual plots. In the velocity versus position graph, the vertical axis represents velocity and the horizontal axis is the direction. Fractures in the obtained graph are due to change from uptrend to downtrend and vice versa at certain points. In the residual plots, horizontal axis represents the number of occurrences of pressure and velocity in X and Y directions, and vertical axis indicates residuals for these parameters. For example, Figures 11 and 12 (a), (b) and (c) illustrate velocity versus position graphs in X and Y directions and the residual plots at Reynolds numbers of 35 and 200, respectively.

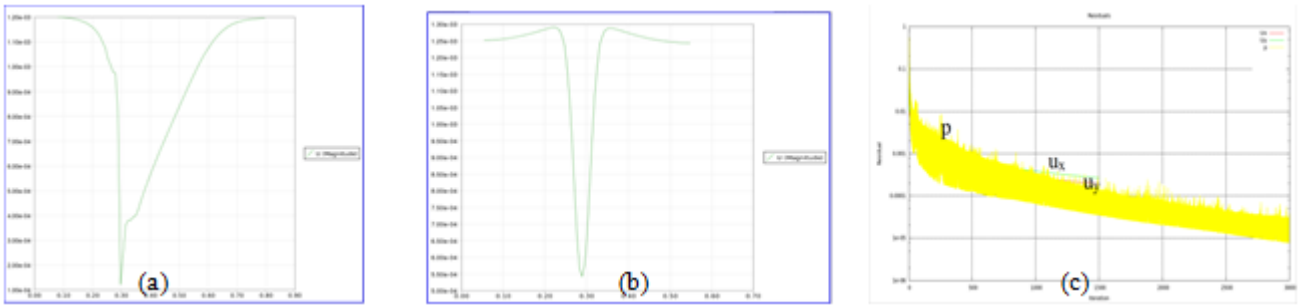

Figure 11- (a) Velocity vs position graphs in X direction. (b) Velocity vs position graphs in Y direction. (c) Residual plot at Reynolds number 35

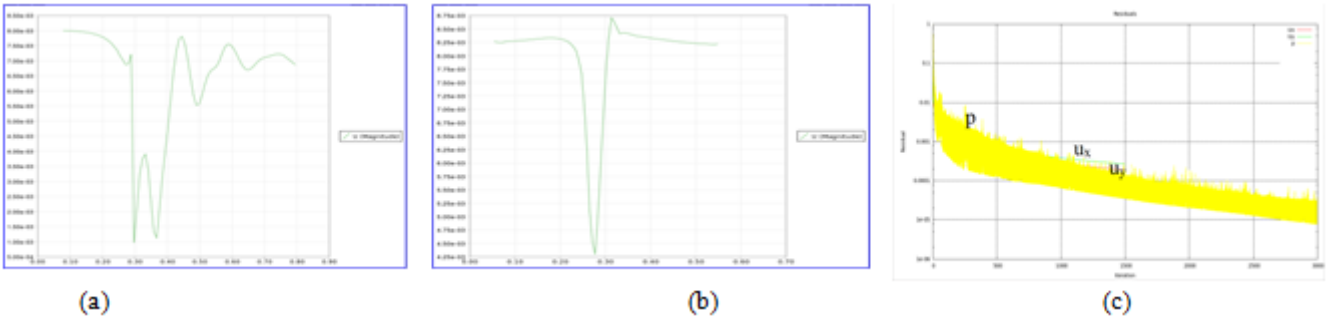

Figure 12- (a) Velocity versus position graphs in X direction. (b) Velocity versus position graphs in Y direction. (c) Residual plot at Reynolds number 200

IV. Conclusions

The present study aimed to investigate flow line patterns behind a triangular obstacle. The results of the first step indicated that size of symmetric vortex pairs depends on the Reynolds number and is changed even with a slight change in this parameter. In the second step, comparisons were performed between vortex patterns in six different times with time step T= 6 at Reynolds numbers of 150 and 200. At 50s, in both conditions no flow line separation occurred and the same flow line pattern was observed in both conditions. At 100s, symmetric vortex pairs were observed in both conditions. At 150 s, flow line patterns were different in the two conditions. At 200, 250 and 300 s, flow line patterns were almost the same for flow line separation and alternative recirculation zone. The results of the third step indicated that flow line pattern changes by changing the Reynolds number, and the increase of the Reynolds number changes flow lines from laminar to turbulent.

Acknowledgement

This work is supported by the Ramin Agriculture and Natural Resources University of Khuzestan, Iran.

References

[1] Bernitsas M.M., Raghavan K., Ben-Simon Y., Garcia E.M.H. VIVACE (Vortex Induced Vibration Aquatic Clean Energy): A new concept in generation of clean and renewable energy from fluid flow. Journal of Offshore Mech. Arct, Vol. 130(4) (2008) 1- 18.

[2] Barrero-Gil A., Pindado S., Avila, S. Extracting energy from Vortex-Induced Vibrations: A parametric study. Journal of Applied Mathematical Modelling, Vol. 36(7) (2012) 3153-3160.

[3] Rajani B.N., Gowda R.V.P., Ranjan P. Numerical Simulation of Flow past a Circular Cylinder with Varying Tunnel Height to Cylinder Diameter at Re 40. International Journal Of Computational Engineering Research (ijceronline.com), 3(1) (2013) 188- 194.

[4] Wei W., Bernitsas M. M., Maki K. Rans simulation versus experiments of flow induced motion of circular cylinder with passive turbulence control at 35,000<Re<130,000. Journal of Offshore Mechanics and Arctic Engineering, 136 (4) (2014) 1-10.

[5] Roohi E., Pendar M. R., Rahimi A. Simulation of three-dimensional cavitation behind a disk using various turbulence and mass transfer models. Journal of Applied Mathematical Modelling 40 (2016) 542–564.

[6] Luo S.C. and Tan R.X.Y. Induced parallel vortex shedding from a circular cylinder at Re $O(10^4)$ by using the cylinder end suction technique. Journal of Experimental Thermal and Fluid Science, 33 (8) (2009) 1172-1179.

[7] Belloli M., Giappino S., Morganti S., Muggiasca S., Zasso A. Vortex induced vibrations at high reynolds numbers on circular cylinders. Journal of Ocean Engineering, Vol. 94 (2015) 140-154.

[8] De A.K. and Dalal A. Numerical simulation of unconfined flow past a triangular cylinder. International Journal for Numerical Methods in Fluids, 52 (7) (2006) 801-821.
[9] Wanderley J.B.V., and Soares L.F.N. Vortex- induced vibration on a two- dimensional circular cylinder with low Reynolds number and low mass-damping parameter. Journal of Ocean Engineering, 97 (2015) 156-164.
[10] Rao K.M. and Manur A.G. Modeling of vortex induced vibration Based hydrokinetic energy converter. Journal of Electrical and Electronics Engineering, Vol. 6(6) (2013) 26-31.
[11] Defina A. and Pradella I. Vortex-induced cross-flow seiching in cylinder arrays. Journal of Advances in Water Resources, 71 (2014) 140-148.
[12] Badhurshah R. and Samad A. Multiple surrogate based optimization of a bidirectional impulse turbine for wave energy conversion. Journal of Renewable Energy, 74 (2015) 749-760.
[13] Tongphong W. and Saimek S. The design and development of an oscillating water turbine. Journal of Energy Procedia, 52 (2014)552-558.
[14] Okuhara S., Takao M., Takami A., Setoguchi, T. Wells turbine for wave energy conversion. Journal of Fluid Dynamics, 3 (2A) (2013) 36-41.
[15] Setoguchi T., Santhakumar S., Maeda H., Takao M., Kaneko K. A review of impulse turbines for wave energy conversion. Journal of Renewable Energy. 23 (2) (2001) 261-292.
[16] Zenklusen A., Walse S., Rohr P.R.v. Influence of ligament shape and thickness on vortex shedding in highly porous structures. Journal of Chemical Engineering Science, 129 (2015) 1-8.
[17] Ding L., Zhang L., Wu C., Mao X., Jiang D. Flow induced motion and energy harvesting of bluff bodies with different cross sections. Journal of Energy Conversion and Management, 91 (2015) 416-426.
[18] Jafari A., Ghomeshi M., Bina M., Kashefipour S.M. Comparing of ten modes of oscillation occurring across the open channels. IAHR-APD congress, The school of engineering, The university of Auckland Newzealand, 21-24 (2010).
[19] Jafari A., Ghomeshi M., Bina M., Kashefipour S.M. Experimental study on ten modes of transverse waves due to vertical cylinders in open channels. Journal of Food, Agriculture and Environment, Vol. 8(2) (2010) 949- 955.
[20] Ghomeshi A.A., Ghomeshi M., Azizi, R., Hooshmand A.R. Experimental investigation on wavelength and frequency of transverse waves from vortex shedding in open channels. International Fluid Dynamics Conference, Shiraz University, Iran.
[21] Blevins R. D. Flow-induced vibration. 2nd edn. New York, Van Nostrand Reinhold, (1990) 471.
[22] Harris C.M. and Piersol A.G. 2002. Harris' shock and vibration handbook. New York, McGraw-Hill, (2010) 1456.
[23] Leinhard J.H. Synopsis of lift, drag, and vortex frequency data for rigid cylinders. Published by Technical Extension Service, Washington State University, (1966) 36.
[24] Williamson C.H.K. and Govardhan R. Vortex-Induced Vibrations. Annu. Rev. Fluid Mech, 36 (2004) 413- 455.
[25] Roshko A. Perspectives on bluff body aerodynamics. Journal of Wind Engineering & Industrial Aerodynamics, 49 (1993) 79–100.
[26] You D., Choi H., Choi M.R., Choi M., Kang S.H. Control of flow induced noise behind a circular cylinder using splitter plates. AIAA Journal, Vol. 36(11) (1998) 1961–1967.
[27] Bovand M., Rashidi S., Dehghan M., Esfahani J. A., Valipour M. S. Control of wake and vortex shedding behind a porous circular obstacle by exerting an external magnetic field. Journal of Magnetism and Magnetic Materials, 385 (2015) 198–206.
[28] Chen Y. and Shao C.P.S. Suppression of vortex shedding from a rectangular cylinder at low Reynolds numbers. Journal of Fluid and Structures, 43 (2013) 15-27.
[29] Dipankar A., Sengupta T.K., Talla S. Suppression of vortex shedding behind a circular cylinder by another control cylinder at low Reynolds numbers. Journal of Fluid Mech, (2006) 1-20.
[30] Zhou L., Cheng M., Hung K.C. Suppression of fluid force on a square cylinder by flow control. Journal of Fluids and Structures, 21 (2005) 151-167.
[31] Mittal S. and Raghuvanshi A. Control of vortex shedding behind circular cylinder for flows at low Reynols numbers. International Journal for Numerical Methods in Fluids, 35 (4) (2001) 421-447.
[32] Perumal D.A., Kumar G.V.S. Dass A.K. Lattice Boltzmann simulation of flow over a circular cylinder at moderate Reynolds numbers. Journal of Thermal Science, Vol. 18(4) (2014) 1235-1246.
[33] Abdolahi M. and Atefi GH. Simulation of vortex shedding phenomena in a two-dimensional flow around a square obstacle in a channel, using the lattice Boltzmann method. Journal of Aerospace mechanics (fluid mechanics and aerodynamics), Vol. 7 (4) (2011) 51-63.
[34] Miguel Darío Ortega López, Exploring and envisioning periodic laminar flow around a cylinder. Master Thesis. 210p. Virginia, Faculty of the Virginia Polytechnic (2009).
[35] Engelbreth K.I. Viscous flow around a circular cylinder near a Plane wall. 113p. Master Thesis, Norwegian (University of Science and Technology (NTNU)) (2011).